[Tectonics]

Supporting Information for

From the seismic cycle to long-term deformation: linking seismic coupling and Quaternary coastal geomorphology along the Andean Megathrust

M. Saillard[1], L. Audin[2], B. Rousset[2], J.-P. Avouac[3], M. Chlieh[1], S. R. Hall[4], L. Husson[2], D. L. Farber[5,6]

[1] Université Côte d'Azur, IRD, CNRS, Observatoire Côte d'Azur, Géoazur, 250 rue Albert Einstein, Sophia Antipolis 06560 Valbonne, France.

[2] IRD, Univ. Grenoble Alpes, CNRS, ISTerre, F-38041 Grenoble, France.

[3] Tectonics Observatory, Division of Geological and Planetary Sciences, California Institute of Technology, Pasadena, CA, 91125, USA.

[4] College of the Atlantic, Bar Harbor, ME 04609, USA.

[5] University of California, Santa Cruz, Santa Cruz, CA, 95065, USA.

[6] Lawrence Livermore National Laboratory, LLNL, Livermore, CA 94550, USA.

Contents of this file

Additional Supporting Information (Files uploaded separately)

Introduction

Here, we present data used in Figure 1a and 1c that have been collected from existing literature: Quaternary uplift rates deduced from marine terraces from central Peru to southern Chile and the major historical earthquakes (Mw≥7.5) for the last 500 yrs. Additional information about the inversion of GPS data for the coupling model and comparison between short-term, GPS-derived interseismic coupling (from *Métois et al.* [2016]) and trench-coast distance are also included.

Site Name		Latitude (degrees)	Uplift rate (m/ka)	±	MIS	References
Arauco Peninsula	Arauco peninsula	-37,49	1,60	0,23	5e	*Melnick et al., 2009*
	Arauco peninsula	-37,73	1,71	0,16	7e	
	Arauco peninsula	-37,57	1,42	0,10	9c	
Altos de Talinay	Altos de Talinay	-30,80	0,18	0,05	5e	*Saillard et al., 2009*
	Altos de Talinay	-30,80	0,28	0,04	7e	
	Altos de Talinay	-30,80	0,52	0,08	9c	
	Altos de Talinay	-30,80	0,64	0,04	17	
Tongoy / Guanaqueros bays	Tongoy	-30,25	0,09	0,04	5e	*Saillard, 2008; Saillard et al., 2012*
	Tongoy	-30,25	0,12	0,03	11	
	Guanaqueros	-30,20	0,33	0,12	5c	*Radtke, 1987*
Coquimbo	Herradura	-30,00	0,12	0,05	5e	*Radtke, 1989*
	Herradura	-30,00	0,16	0,05		*Leonard and Wehmiller, 1992*
	North Coquimbo Bay	-29,90	0,18	0,07		*Leonard and Wehmiller, 1992*
	Punta teatinos	-29,80	0,22	0,05		*Radtke, 1989*
	Herradura	-30,00	0,20	0,03	7e	*Radtke, 1989*
	Punta teatinos	-29,80	0,31	0,03		
	South Coquimbo Bay	-30,00	0,08	0,03	9c	*Leonard and Wehmiller, 1992*
	Herradura	-30,00	0,10	0,04	11	*Leonard and Wehmiller, 1992*
	North Coquimbo Bay	-29,90	0,14	0,04		
	Quebrada Honda	-29,60	0,17	0,05	5e	*Radtke, 1987*
	Huasco	-28,30	0,22	0,07	5e	*Radtke, 1987*
Bahia Inglesa / Caldera	Puerto Viejo	-27,33	0,45	0,13	5c	*Radtke, 1987*
	Bahia Inglesa	-27,12	0,30	0,12		
	Caldera	-27,06	0,38	0,12		
	Puerto Viejo	-27,33	0,43	0,07	5e	*Radtke 1987*
	Bahia Inglesa	-27,12	0,27	0,07		
	Bahia Inglesa	-27,06	0,34	0,05	11	*Marquardt et al., 2004*
	Caldera	-27,12	0,40	0,05		
	Morro de Copiapo	-27,10	0,26	0,06	13	*Leonard et al., 1994*
	Caldera	-27,15	0,26	0,02	21	*Quezada et al., 2007*
	Obispito	-26,45	0,26	0,09	5e	*Radtke, 1987*
	Pan de Azucar	-26,15	0,25	0,05	5e	*Radtke, 1987*
	Cifuncho	-25,65	0,25	0,04	5e	*Radtke, 1989*
Mejillones Peninsula	Hornitos	-22,90	0,48	0,13	5c	*Ortlieb et al., 1996a*
	Coloso	-23,75	0,12	0,04	5e	*Radtke, 1989*
	Mejillones north	-23,05	0,09	0,03		*Radtke, 1989*
	Chacaya	-23,00	0,25	0,05		*Ortlieb et al., 1996a*
	Hornitos	-22,90	0,27	0,04		*Radtke, 1989*
	Hornitos	-22,90	0,25	0,05		*Ortlieb et al., 1996a*
	Hornitos	-22,90	0,25	0,05		*Radtke, 1989; Ortlieb et al., 1996a*
	Coloso	-23,75	0,18	0,03	7e	*Radtke, 1989*
	Abtao	-23,45	0,13	0,04		*Radtke, 1989*
	Abtao	-23,45	0,14	0,04		*GEOTOP unpublished*
	Mejillones north	-23,05	0,18	0,03		*Radtke, 1989*
	Chacaya	-23,00	0,43	0,06		*Ortlieb et al., 1996a*
	Hornitos	-22,90	0,26	0,03		*Radtke, 1989*
	Hornitos	-22,90	0,28	0,06		*Radtke, 1989; Ortlieb et al., 1996a*
	Abtao	-23,45	0,27	0,05	9c	*GEOTOP unpublished*
	Mejillones north	-23,05	0,13	0,05		*Radtke, 1989*
	Chacaya	-23,00	0,27	0,05		*Ortlieb et al., 1996a*
	Hornitos	-22,90	0,24	0,03		*Ortlieb et al., 1996a*
	Morro Mejillones	-23,10	0,62	0,08	11	*Gonzalez, after Marquardt, 2005*
Michilla	Michilla	-22,70	0,30	0,04	5e	*Leonard and Wehmiller 1991*
	Michilla	-22,70	0,18	0,11		*GEOTOP unpublished*
	Michilla	-22,70	0,39	0,11		*Labonne and Hillaire-Marcel, 2000; Leonard and Wehmiller, 1991*
	Iquique	-20,40	0,16	0,04	5e	*Radtke, 1989*
Ilo	Ilo	-17,60	0,29	0,15	5a	*Ortlieb et al., 1992; Ortlieb et al., 1996b*
	Ilo	-17,70	0,14	0,07	5e	*Ortlieb et al., 1992*
	Ilo	-17,70	0,15	0,04	7e	*Ortlieb et al., 1992; Ortlieb et al., 1996b*
	Ilo	-17,58	0,24	0,02	9c	*Saillard, 2008*

	Ilo	-17,70	0,18	0,06		*Ortlieb et al., 1996b*
Chala / Tanaka / Chaviña	Chala	-15,85	0,47	0,06	5e	*Saillard, 2008*
	Chala	-15,85	0,45	0,03	7e	
	Tanaka	-15,74	0,43	0,06		
	Chala	-15,85	0,47	0,03	9c	
	Chaviña	-15,60	0,46	0,05		
	Chala	-15,85	0,46	0,04	11	*Goy et al., 1992*
		-15,50	0,68	0,04	7e	*Osmond, 1987*
San Juan de Marcona	Cerro El Huevo	-15,30	0,71	0,08	5a	*Saillard et al., 2011*
		-15,30	0,87	0,07	5c	
		-15,30	0,82	0,08	5e	
		-15,30	0,70		5e	*Macharé and Ortlieb, 1992*
		-15,30	0,70	0,04	7e	*Saillard et al., 2011*
		-15,30	0,63	0,03	9a	
		-15,30	0,59	0,03	9c	
		-15,30	0,55	0,04	11	
		-15,30	0,47		11	*Hsu, 1992*
	Cerro Tres Hermanas	-15,37	0,70	0,08	5a	*Saillard et al., 2011*
		-15,37	0,69	0,08	5c	
		-15,37	0,61	0,09	5e	
		-15,37	0,61	0,03	7e	
		-15,37	0,54	0,03	9a	
		-15,37	0,49	0,02	9c	
		-15,37	0,44	0,03	11	

Table S1. Uplift rates of marine terraces available in the literature and used in Figure 1d from southern Chile to southern Peru (modified from *Regard et al.* [2010]). For graphical clarity reasons, we picked the highest uplift rates (in dark) when several data were available for a same site. Data in grey were not reported in Figure 1d but are shown for information.

Date	Source	Location	Magnitude	Length
12/16/1575	Lomnitz, 2004	Southern Chile	8.5	>500
02/08/1570	Lomnitz,1970	Southern Chile	8.3	180
08/15/1582	Dorbath et al., 1990	SouthernPeru	7.5	75
07/09/1586	Watanabe, 1983	Central Peru	8.1	80
11/24/1604	Dorbath et al., 1990	SouthernPeru	8.7	450
05/13/1647	Beck et al.,1998	Southern Chile	8.5	380
03/15/1657	Lomnitz,1970	Southern Chile	8	190
10/20/1687	Beck and Nishenko, 1990	Central Peru	8.6-8.7	>300
1715	Dorbath et al., 1990	Central Peru	7.5	75
07/08/1730	Beck et al., 1998	Southern Chile	8.7	550
12/24/1737	Lomnitz,1970	Southern Chile	7.7	>500
10/28/1746	Spence et al.,1999	Central Peru	8.6-9.5	350
05/25/1751	Cisternas et al., 2005	Southern Chile	8.5	500
06/25/1784	Dorbath et al., 1990	Central Peru	8.4	300
03/30/1796	Comte et al., 2002	Northern Chile	7.7	~200
04/11/1819	Comte et al., 2002	Southern Chile	8.3	300
11/19/1822	Lomnitz, 2004	Southern Chile	8-8.5	220
1833	Dorbath et al., 1990	Central Peru	7.2-7.7	50-100
02/20/1835	Lomnitz, 2004	Southern Chile	8.5	200
11/07/1837	Cisternas et al., 2005	Southern Chile	8.5	500
10/05/1859	Comte et al.,2002	Central Chile	7.6	100
13/08/1868	Spence et al., 1999	SouthernPeru	8.8	400
10/05/1877	Spence et al., 1999	Northern Chile	8.8	400
08/15/1880	Beck et al., 1998	Southern Chile	7.7	150
08/17/1906	Melnick et al., 2006	Central Chile	8.6	340
06/08/1909	Comte et al., 2002	Central Chile	7.6	~100
08/06/1913	Dorbath et al., 1990	Central Peru	7.8	<100
05/20/1918	Comte et al., 2002	Northern Chile	7.9	?
12/04/1918	Comte et al., 2002	Northern Chile	8.2	110
11/10/1922	Kelleher, 1972	Central Chile	8.4	390
12/01/1928	Lomnitz, 1970	Southern Chile	8.4	?
01/25/1939	Lomnitz, 2004	Southern Chile	8.3	190
05/24/1940	Beck and Nishenko, 1990	Central Peru	8	180
08/24/1942	Giovanni et al., 2002	Central Peru	8.1	210
04/06/1943	Kelleher, 1972	Central Chile	8.3	210
08/02/1946	Comte et al., 2002	Northern Chile	7.9	?
05/24/1960	Cisternas et al., 2005	Southern Chile	9.5	700
10/17/1966	Dorbath et al., 1990	Central Peru	8.2	100
05/31/1970	Dorbath et al., 1990	Central Peru	7.7	150
07/08/1971	Comte et al., 1986	SouthernPeru	7.9	110
10/03/1974	Beck and Nishenko, 1990	Central Peru	8.1	280
03/03/1985	Comte et al., 1986	Central Chile	7.8	170
07/30/1995	Delouis et al., 1997	Northern Chile	8.1	200
11/12/1996	Giovanni et al., 2002	Central Peru	7.7	130
02/21/1996	Bilek, 2010	Central Peru	7.5	110
06/23/2001	Giovanni et al., 2002	SouthernPeru	8.5	300
07/07/2001	Giovanni et al., 2002	SouthernPeru	7.6	-
08/15/2007	Perfettini et al., 2010	Central Peru	8	160
11/14/2007	Bilek, 2010	Northern Chile	7.7	160
02/27/2010	Moreno et al., 2010	Southern Chile	8.8	500
04/01/2014	Ashtari Jafari, 2015	Northern Chile	8.2	~120
04/04/2014	Ashtari Jafari, 2015	Northern Chile	7.7	~120
09/16/2015	Ruiz et al., 2016	Central Chile	8.3	~230

Table S2. Major historical earthquakes (Mw≥7.5) that ruptured the plate interface in the trench-parallel direction from central Peru to southern Chile for the last 500 years and used in Figure 1b (for Mw≤7.5, see Barrientos, 2007).

Supplementary information 1:

GPS data selection

To model the interseismic coupling pattern along the megathrust interface, we compiled published interseismic GPS data collected between 1993 and 2013. In Peru, we used the GPS compilation of *Chlieh et al.* [2011] that includes data from *Norabuena et al.* [1998], *Bevis et al.* [2001], *Gagnon et al.* [2005]. In Chile, we used the GPS data from *Brooks et al.* [2011], *Moreno et al.* [2011] and *Métois et al.* [2013, 2014] that includes data from *Métois et al.* [2012], *Ruegg et al.* [2009] and *Vigny et al.* [2009]. In areas affected by recent great megathrust earthquakes (i.e., 2001 Arequipa, 2007 Pisco and Tocopilla, 2010 Maule, 2014 Pisagua and 2015 Illapel), we choose the interseismic GPS velocities preceding these events to avoid displacement signals related to co- and post-seismic transients. The resulting compilation is a selection of 300 interseismic GPS measurements referenced to a common stable South America reference frame in ITRF2008 [*Altamimi et al.,* 2011].

GPS-derived interseismic coupling model.

To produce the interseismic coupling pattern along the megathrust interface described in the main text, we performed non-linear inversions of the GPS data based on a simulated annealing algorithm to determine the interseismic coupling distribution [*Chlieh et al.,* 2011]. Two types of constraints were used: one that minimizes the misfit (wrms) and a second that minimizes the difference in slip between adjacent subfaults. Two weights W_{st} and W_c are used to adjust the trade-off between fitting the data sets and satisfying the constraints. The criteria to invert the geodetic observations is represented as:

$$W_{st} \,.\, err_{st} + W_c \,(\text{constraints}) = \text{minimum} \qquad (1)$$

All inversions start with random initial fault models. The inversions of individual datasets with no constraints are first performed to determine the maximum improvements, which are then used to normalize the err_{st} in the refined inversions. The smoothing constraints are also normalized with the value of the initial models. After this processing, the weights W_{st} and W_c become dimensionless and equation (1) can be written as the weighted quadratic summation of the misfit to the data and a term that control the roughness of the distribution:

$$\text{Cost} = \text{wrms}^2 + \lambda_1 \, \text{Dc}^2 \qquad (2)$$

Dc represents the differences in back-slip rate between adjacent cells and a factor λ_1 that controls the smoothing of the distribution through a L1+L2 norm [*Ji et al.*, 2002]. We searched for the optimal smoothing factors by varying λ_1 from 0.001 to 100 and found that the best GPS-fitting model family is for $0.1<\lambda_1<1$. Figure S1 reports the interseismic coupling model for $\lambda_1=0.5$ and the GPS residuals are all within their formal error ellipses. The misfit (wrms) for this model is 3.2 mm/yr.

Spatial Resolution test

Using the spatial distribution and uncertainties of the GPS sites compiled for Peru and Chile, along with the slab geometry described in the main text, we performed a spatial resolution test to emphasize areas that are well resolved. We defined an initial checkerboard model with typical cell size of 120 km x 60 km (Figure S2). The initial checkerboard is expressed in term of characteristic size heterogeneities of full locking (shown in red in Figure S2) and full creeping (in white, Figure S2). The spatial resolution is high in regions where the density of observations is important and drops off significantly where observations are missing. In Peru, the resolution is globally high below the coastline but falls significantly near the trench, especially where the trench-coast distance is the highest. Along the Chilean trench, the along-strike resolution is relatively high nearly everywhere except between 25°S and 26°S and south of latitude 39°S.

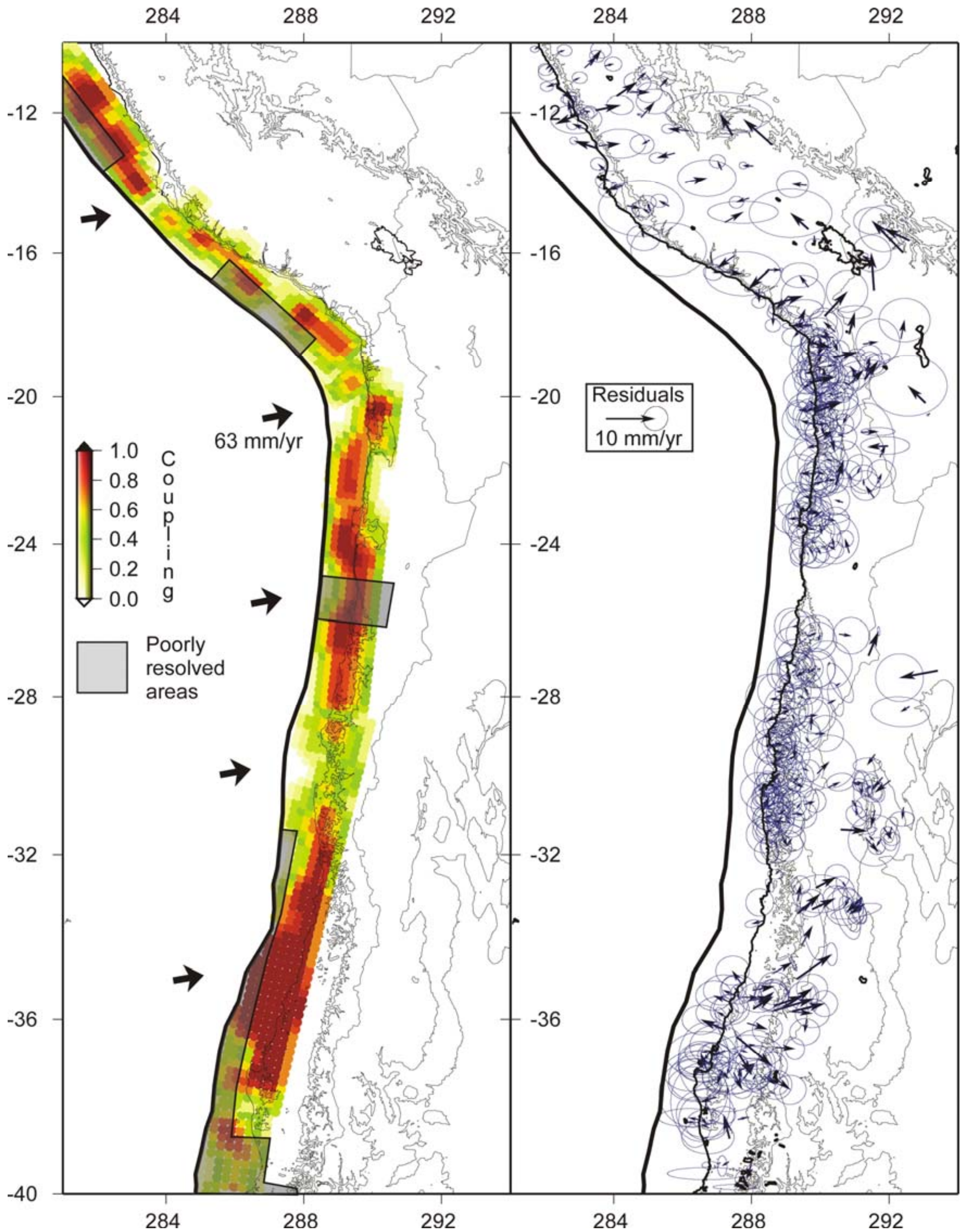

Figure S1. On the left, Interseismic coupling map produced from the inversion of the GPS sites. The misfit (wrms) for this model is 3.2 mm/yr. On the right, GPS residuals (observed – modelled) with their formal 95% confidence level error ellipses.

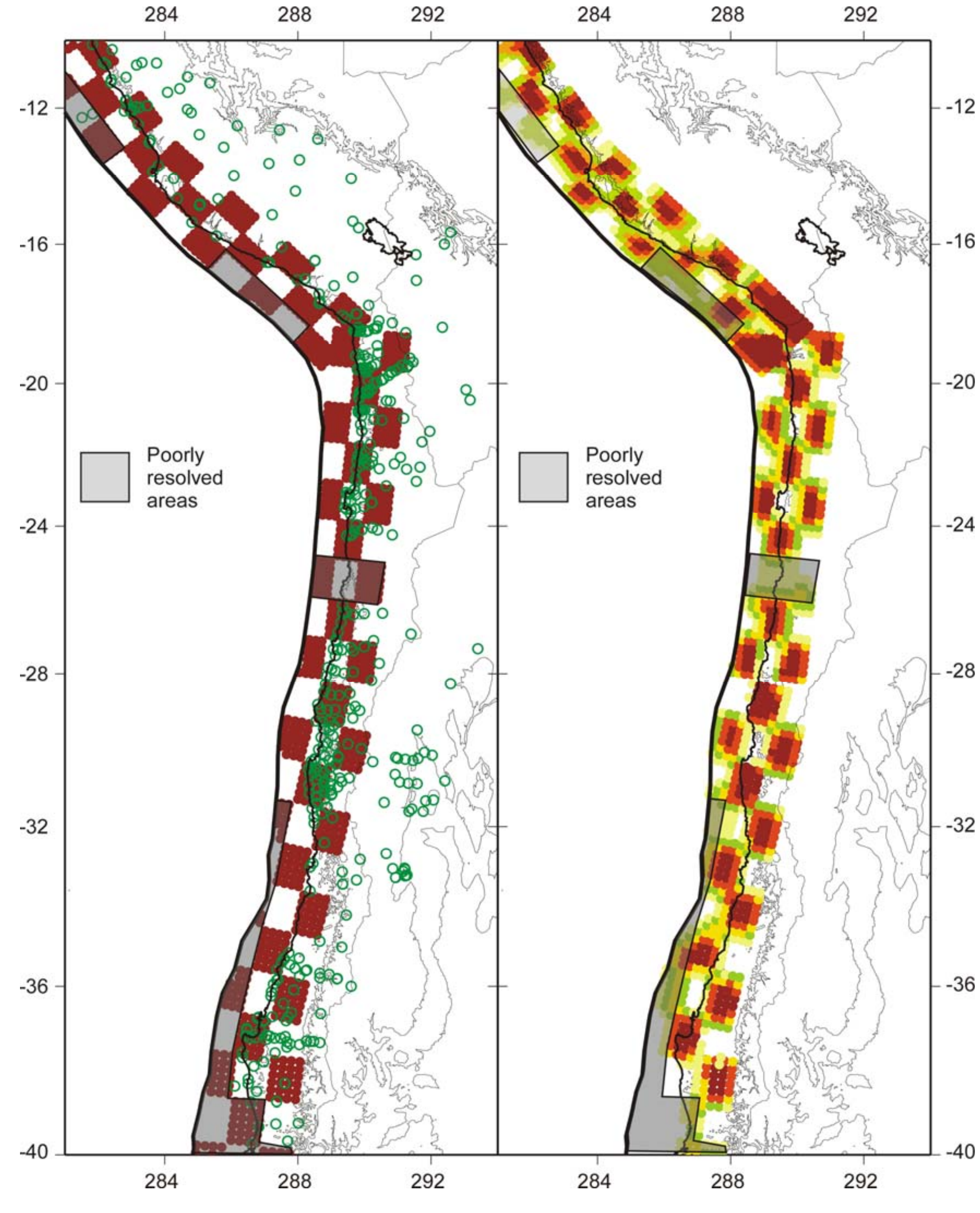

Figure S2. Spatial resolution of the interseismic coupling along the megathrust interface. On the left, initial checkerboard model used to compute forward displacements at each GPS sites (green circles). Red patches have a surface of 120 km (along-strike) x 60 km (along-dip) and are considered fully locked. On the right, inverted solution considering the same input parameters (slab geometry, rake direction, smoothing coefficient). Most of the initial patches are reconstructed suggesting areas of high spatial resolution. Poorly defined or missing patches correspond to areas of the megathrust that are poorly resolved (grey shaded areas).

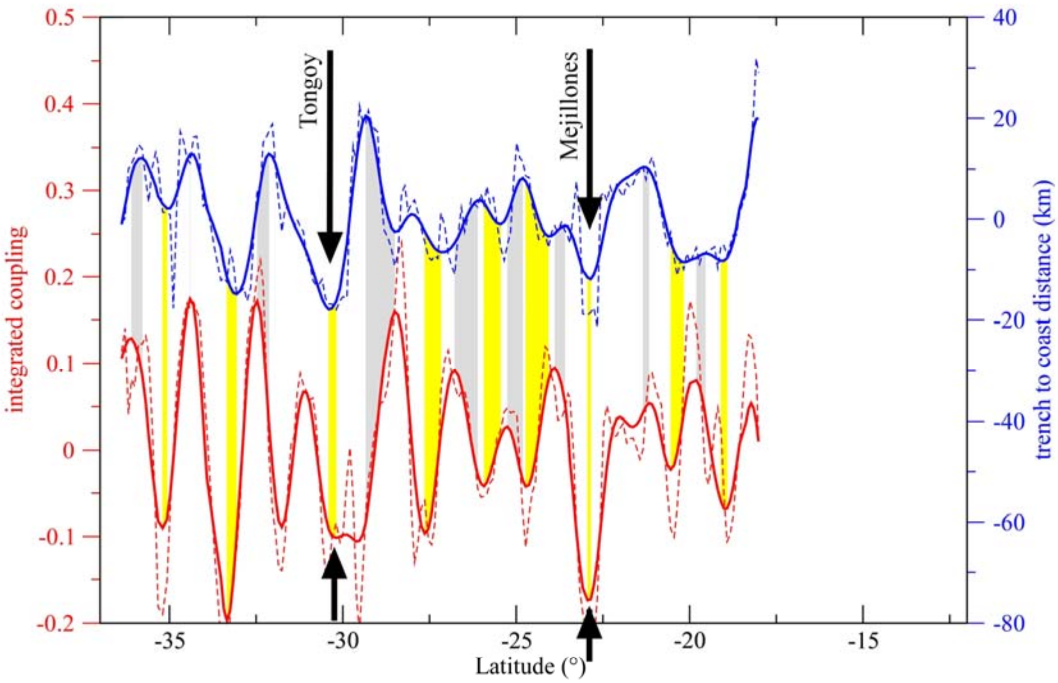

Figure S3. Comparison between short-term, GPS-derived interseismic coupling (red) and trench-coast distances (blue) integrated along the Benioff zone in the convergence direction (Euler pole from NUVEL1A, [*DeMets et al.,* 1994]). Both signals have been band-passed for wavelengths ranging between 100 km and 500 km (including the mean values, and therefore represent departures from average). Dashed lines show the high-pass filtered signal, leaving all wavelengths shorter than 500 km. Coupling is integrated downdip along the convergence directionmodeled by *Métois et al.* [2016] (http://perso.univ-lyon1.fr/marianne.metois/docs/average_coupling_bestmod.txt) and projected on the slab geometry derived by *Hayes et al.* [2012]. Black arrows indicate the location of the main peninsulas. Color bars indicate the shortest width pairs of minima (peninsulas and low coupling areas, yellow; embayments and high coupling areas, gray).